(This is a sample cover image for this issue. The actual cover is not yet available at this time.)

Remote Sensing of Environment 127 (2012) 14–29

Contents lists available at SciVerse ScienceDirect

Remote Sensing of Environment

journal homepage: www.elsevier.com/locate/rse

Snow depth and snow water equivalent estimation from AMSR-E data based on *a priori* snow characteristics in Xinjiang, China

Liyun Dai [a,b], Tao Che [a,*], Jian Wang [a], Pu Zhang [c]

[a] Cold and Arid Regions Environmental and Engineering Research Institute, Chinese Academy of Sciences, Lanzhou 730000, China
[b] Graduate University of Chinese Academy of Sciences, Beijing 100049, China
[c] Urumqi Meteorological Satellite Ground Station, Urumqi 830002, China

ARTICLE INFO

Article history:
Received 15 February 2012
Received in revised form 8 August 2012
Accepted 11 August 2012
Available online xxxx

Keywords:
Snow depth
Snow water equivalent
Passive microwave
Look-up table

ABSTRACT

Static snow depth retrieval algorithms tend to underestimate the snow depth at the beginning of the snow season and overestimate the snow depth at the end of the snow season because the snow characteristics vary with the age of snow cover. A novel snow depth/water equivalent (SWE) data retrieval algorithm from passive microwave brightness temperature is proposed based on *a priori* snow characteristics, including the grain size, density and temperature of the layered snowpack. The layering scheme was established based on the brightness temperature difference (TBD) at two different frequencies, which indicates volume scattering, whereas the snow grain size and density of each layer were parameterized according to the age of the snow cover, and the snow temperature and temperature at the snow/soil interface were determined by the air temperature and snow depth. Furthermore, the microwave emission model of layered snowpacks (MEMLS) was used to simulate the brightness temperature at 10 GHz, 18 GHz and 36 GHz based on the *a priori* snow characteristics including snow grain size, density, depth and snow layering. Finally, three look-up tables (one layer, two layers and three layers) were generated for each day, which represent the relationship between the brightness temperatures at 10 GHz, 18 GHz and 36 GHz and snow depth. To avoid underestimation caused by the saturation of the microwave signal at 36 GHz, the TBD1 (the difference of brightness temperature at 18 and 36 GHz) was used to estimate the snow depth if TBD1 was less than 40 K, and TBD2 (the difference of the brightness temperature at 10 and 18 GHz) was used if TBD1 was greater than 40 K. The snow depth and SWE determined by this new algorithm were validated by snow measurements at thirteen meteorological stations in Xinjiang, China from 2003 to 2010 and compared with existing SWE products from the National Snow and Ice Data Center (NSIDC), the Environmental and Ecological Science Data Center for West China (WESTDC), the European Space Agency (ESA) and measurements with a snow course. The results showed that the root mean squared error (RMSE) and the bias from this new algorithm were greatly reduced compared to NSIDC, moderately reduced compared to ESA and slightly reduced compared to WESTDC. The understanding of *a priori* local snow characteristics can improve the accuracy of snow depth and snow water equivalent estimation from passive microwave remote sensing data.

1. Introduction

Seasonal snow cover plays an important role in hydrological cycles and climate processes (Simic et al., 2004). Snow depth is a significant parameter in climate and hydrologic model simulations (Dressler et al., 2006; Gong et al., 2007). The successful estimation of the snow water equivalent can improve the accuracy of the snowmelt-runoff prediction and the management of the water supply (Kuras et al., 2008; Tanasienko et al., 2011). The observations of the sparse weather stations are not sufficient for this purpose; therefore, it is important to develop a snow depth or snow water equivalent (SWE) retrieval method from remote sensing data.

At present, passive microwave remote sensing is the most efficient way to derive snow depth at global and regional scales (Derksen et al., 2010; Foster et al., 2009; Saraf et al., 1999; Tedesco and Narvekar, 2010). The current snow depth or SWE retrieval algorithms have been developed based on the fact that deeper snowpacks have lower microwave brightness temperatures and that the brightness temperature difference (TBD) at 18 GHz and 36 GHz increases with increasing snow depth (Chang et al., 1976; Foster et al., 1997). But when the snow depth reach up to a certain threshold, the brightness temperature at 36 GHz begins to increase slowly or keep stable with the increase of snow depth due to the fact that snow depth exceeds the penetration depth of the 36 GHz, resulting to the TBD at 18 GHz and 36 GHz decreases with the increase of snow depth (Tedesco

* Corresponding author at: 320 Donggang West Road, Lanzhou, Gansu, 730000, China. Tel.: +86 931 4967966; fax: +86 931 8279161.
E-mail address: chetao@lzb.ac.cn (T. Che).

0034-4257/$ – see front matter © 2012 Elsevier Inc. All rights reserved.
http://dx.doi.org/10.1016/j.rse.2011.08.029

and Narvekar, 2010). Therefore, when snow depth is more than this threshold, the lower frequencies (such as 10 GHz and 18 GHz) can be used to retrieve snow depth/SWE. In fact, given stable snow depth, the TBD will increase with increasing grain size and decrease with increasing snow density (Che et al., 2011; Foster et al., 2005; Tsang et al., 2000). Therefore, it is necessary to develop an algorithm that accounts for local snow properties (Che et al., 2008; Stankov et al., 2008).

Another problem within these static algorithms is that the snow grain size and density vary during the snow season, and many researchers have attempted to solve this problem. Kelly et al. (2003) used a time-varying approach to derive snow depth, which assumes that the snowpack properties are spatially and temporally variable. Foster et al. (2005) developed a dynamic algorithm based on the algorithm of Chang et al. (1976). In this dynamic algorithm, the effect of the evolution of snow crystals in response to the progression of the snow season is accounted for by using snow crystal information that is based on the classification system for seasonal snow cover proposed by Sturm et al. (1995). In Canada, studies have indicated that this algorithm captures the snow accumulation and ablation phases. In China, effects from the seasonal variations of snow grain size and density were also identified by Che et al. (2008), and a statistical regression method was adopted to adjust the coefficient dynamically based on the error-increasing ratio within the snow season from October to April. Based on the linear regression method, the average offsets can be obtained to remove the influence of snow density and grain size variations for each month within the snow season. In these two modified algorithms, the error coefficient and monthly offset are constants. Tsutsui et al. (2007) used 89 GHz microwave satellite data to estimate changes in snow particles, which is a method based on the assumption that high-frequency microwaves are sensitive to the scattering effect related to the changes in the snow grains. Josberger and Mognard (1998) proposed the temperature gradient index (TGI), which represents the cumulative bulk temperature gradient through the snowpack for the whole of snow season and a cumulative index of the potential for grain size growth through the whole of snow season. Therefore, the TGI can be used to retrieve snow depth by the incorporation of snow grain size growth (Josberger and Mognard, 2002).

Snow stratigraphy is another factor that strongly affects the snow microwave radiative and scattering properties (Durand et al., 2008; Wiesmann and Mätzler, 1999). Layering is inherent to most snowpacks, and the microwave brightness temperature from layered snowpacks can be simulated by microwave radiative transfer models (RTM), such as the microwave emission model of layered snowpacks (MEMLS, Wiesmann and Mätzler, 1999). However, it becomes more difficult to retrieve the snow depth and SWE of a layered snowpack from brightness temperature data because the layered condition is unknown.

Therefore, *a priori* information of snowpacks, including snow grain size, density and stratigraphy, is very helpful in estimating the snow depth and SWE. In this paper, a snow depth/SWE retrieval algorithm of a look-up table was developed based on *a priori* snow characteristics (stratigraphy, snow grain size, density, snow temperature and temperature at the snow/soil interface) in Xinjiang, China. This algorithm uses the MEMLS model to simulate brightness temperature, establishes look-up tables for different types of layered snowpacks and adopts the spectral gradient method (*i.e.*, TBD) to derive snow depth and SWE. The results indicated that the new method can improve the accuracy of snow depth/SWE retrieval over the state-of-the-art in Xinjiang, China. In Section 2, we describe the data used in this paper. Section 3 details the snow depth retrieval method, including the snowpack layering scheme, and the spatiotemporal variations of snow grain size, density, snow temperature and temperature at the snow/soil interface, which are *a priori* information for the establishment of the look-up table. Section 4 analyzes the uncertainties of this method, and in Section 5, the retrieval result and its validation is presented.

2. Data

2.1. Satellite data

We used the Advanced Microwave Scanning Radiometer for Earth Observing System (AMSR-E) data in this study. The AMSR-E instrument was boarded on the NASA EOS Aqua satellite, and it provides global passive microwave measurements of the Earth (Knowles et al., 2006). The EASE-Grid (equal-area scalable earth grid) brightness temperatures (6.9 GHz, 10.7 GHz, 18.7 GHz, 23.8 GHz, 36.5 GHz and 89.0 GHz) have been available from the National Snow and Ice Data Center (NSIDC) since June 2002. In this study, we used the brightness temperatures at 10.7 GHz, 18.7 GHz of horizontal polarization, and 36.5 GHz of both polarizations to retrieve SWE from 2003 to 2010. The brightness temperatures at 10.7 GHz, 18.7 GHz and 36.5 GHz of horizontal polarization were used to retrieve SWE, and that at 36.5 GHz of both vertical and horizontal polarizations were used to identify wet snow. To avoid possible snow-melt effects on brightness temperatures during the day, night-time overpasses (descending orbits, the overpass time is approximately 03:00 am local time) were employed.

2.2. Field experimental data

The Xinjiang province locates on the Northwest of China (Fig. 1). The south and north of Xinjiang are dominated by the grass land, and in the central part, the land cover is mainly the bare ground according to Ran et al. (2012). Regarding the snow-climate class, Xinjiang belongs to the prairie according to Sturm et al. (1995). From November of 2010 to March of 2011, three field measurements were established in Northern Xinjiang, and at the end of February of 2011, snow depths were measured along a snow course (Fig. 1). During the field experiment period, a large number of snow pits were measured in detail, and these measurements included snow depth, grain size, density, snow temperature, temperature at the snow/soil interface and the stratigraphy of snow during different stages of the snow season. Grain diameter is measured by an optical microscope with 80X. Snow density is measured by snow fork which is a portable instrument for measuring the properties of snow. The sensor is a steel fork used as a microwave resonator. Snow Fork measures the electrical parameters: resonant frequency, attenuation and 3-dB bandwidth. The measuring results are used to calculate accurately the complex dielectric constant of snow. Finally, the snow density is calculated using semi-empirical equations.

Take, for example, the six typical records illustrated in Fig. 2, which include two deep snow pits at Fuyun (30 cm) and Jichangcun (60 cm), two medium snow pits at Cainan1 (12 cm) and Shixi (22 cm), and two shallow snow pits in Fukang (3 cm) and Cainan2 (6 cm). According to these field measurements, snow density and averaged grain size can be summarized for the different ages of snow (e.g., new snow, fine snow, densified snow, coarse grain and depth hoar) as shown in Table 1. The snow density and grain size increases from the top down in snowpacks. These data provide the *a priori* local snow information for the development of the new method.

Snow temperature varies with time within one day. The above-mentioned snow pits often were measured during the daytime; however, the AMSR-E brightness temperature at the night-time overpass time was used in this study. There are logistics in Fukang (a), Fuyun (b), Shixi (d) and Jichangcun (e), so it is convenient to measure the snow temperatures profiles at night time (Fig. 1). During the field experiments, snow temperatures profiles at sixteen snow pits were observed around Sites a, b, d and e, which are described in Section 3.1.4.

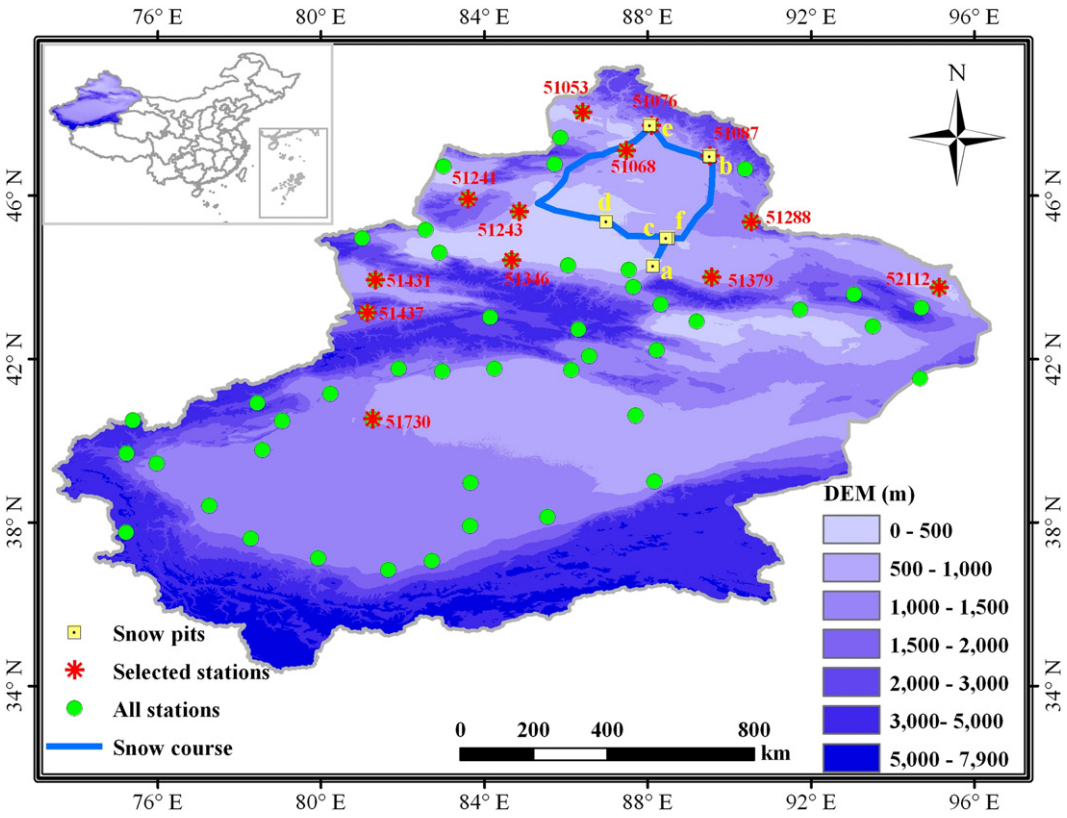

Fig. 1. Route of the snow course, locations of snow pits of snow field measurements, and the distribution of meteorological stations. Green circles are 55 meteorological stations in Xinjiang. Yellow squares (A-F) are snow profile observation sites (for Fukang, Fuyun, Cainan1, Shixi, Jichangcun, Cainan2, respectively). 13 red snowflakes are meteorological stations selected for validation.

2.3. Snow and air temperature observations at meteorological stations

The daily snow depth, snow pressure and minimum air temperature observations from 55 stations in Xinjiang, China, from 1999 to 2008 (several up to 2010) are available from the China Meteorological Administration, and the station locations are illustrated in Fig. 1. Not all stations have complete snow depth and pressure measurements; thus, thirteen stations were selected for further analyses and are marked with red points in Fig. 1.

SWE can be converted from snow pressure by

$$\text{SWE (mm)} = \text{snow pressure } \left(\text{g/cm}^2\right) \times 10/\text{water density } \left(\text{g/cm}^3\right), \quad (1)$$

and snow density can be expressed by

$$\text{snow density } \left(\text{g/cm}^3\right) = \text{snow pressure } \left(\text{g/cm}^2\right)/\text{snow depth (cm)}. \quad (2)$$

These snow density and air temperature data were used in developing the retrieval algorithm, and SWE and snow depth were used to validate the algorithm. In general, the ten-year data from the meteorological stations show that seasonal snow cover appears from the end of October to the beginning of November, reaches its maximum in the end of January and the beginning of February, then rapidly decreases in March and disappears at the beginning of April. However, snow density is lowest at the end of November and slowly increases towards the end of the snow season (March–April), although a slightly higher density occurs at the beginning of the snow season due to the higher air temperature (corresponding to the moist snowfall) (Fig. 3).

3. Algorithm development

In this study, we propose a look-up table method to retrieve snow depth and SWE. First, a look-up table between snow properties and passive microwave brightness temperature at AMSR-E frequencies was established using the microwave emission model of layered snowpacks (MEMLS) based on *a priori* snow characteristics, which come from field measurements and meteorological station data (Fig. 4). These *a priori* snow characteristics include snow grain size, snow density, snow temperature, temperature at the snow/soil interface, snow layering and the internal relationships and their variations within a snow season. The determination of each variable or parameter will be described individually in Section 3.1.

For the retrieval of snow depth and SWE, the TBD was used instead of the brightness temperature data at each frequency because TBD can reduce the influences of the atmosphere, underlying ground and snow temperatures (Chang et al., 1976). The retrieval process is illustrated in Fig. 5 and will be explained in Section 3.2.

3.1. Establishment of look-up tables

The microwave emission model of layered snowpacks (MEMLS) can calculate the brightness temperature that is radiated from multilayered snowpacks (Wiesmann and Mätzler, 1999). The MEMLS model requires eight variables and three parameters to simulate the brightness temperature of snowpacks. The three parameters are frequency, incidence angle and polarization, which are provided by the AMSR-E instrument, whereas the eight variables include snow thickness, density, correlation length, temperature, liquid water content, the salinity of each layer and the brightness temperature from the underlying ground and sky background. For the brightness temperature from the underlying ground, we assume that the ground soil is frozen

in snow season and that its emissivity is approximately 0.93 at the horizontal polarization, which is the polarization that is used in the retrieval algorithm, whereas the ground physical temperature is equal to the temperature at the snow/soil interface. The brightness temperatures of the sky background are 5, 15 and 25 K at 10.7, 18.7 and 36.5 GHz, respectively (Qiu et al., 2010; Rose, 2009). The liquid water content within the snowpack is assumed to be zero because only night-time overpass brightness temperature data will be used. The salinity is also assumed to be zero. Therefore, only the snow depth, density, correlation length and snow temperature of each layer must be determined.

3.1.1. Snow layering

According to the field measurements, we argue that the snow cover can reach as many as three layers. At the upper layer, the snow is fresh and loose with low density and small grain size characteristics. In the bottom snow layer, the snow is old and often undergoes compaction due to the overburden and freeze/thaw cycle, which leads to a larger grain size and higher density. However, the increasing rate of snow density growth from the upper to the bottom snow layer is lower than the rate of grain size growth due to the depth hoar phenomenon. In the middle snow layer, the grain size and density are intervenient of the upper and bottom layers. In fact, when snow is shallow, there may be only one or two snow layers. Although one or two interlayers can occasionally appear within some snowpacks, this study only focus on these typical snow properties described above.

Therefore, snow depth is used to determine the number of snow layers. When the snow depth is greater than 20 cm, snow cover is often characterized as three layers, whereas when the snow depth is less than 10 cm, it has the characteristics of the upper snow layer (one layer). For the case of three snow layers, the thicknesses of the

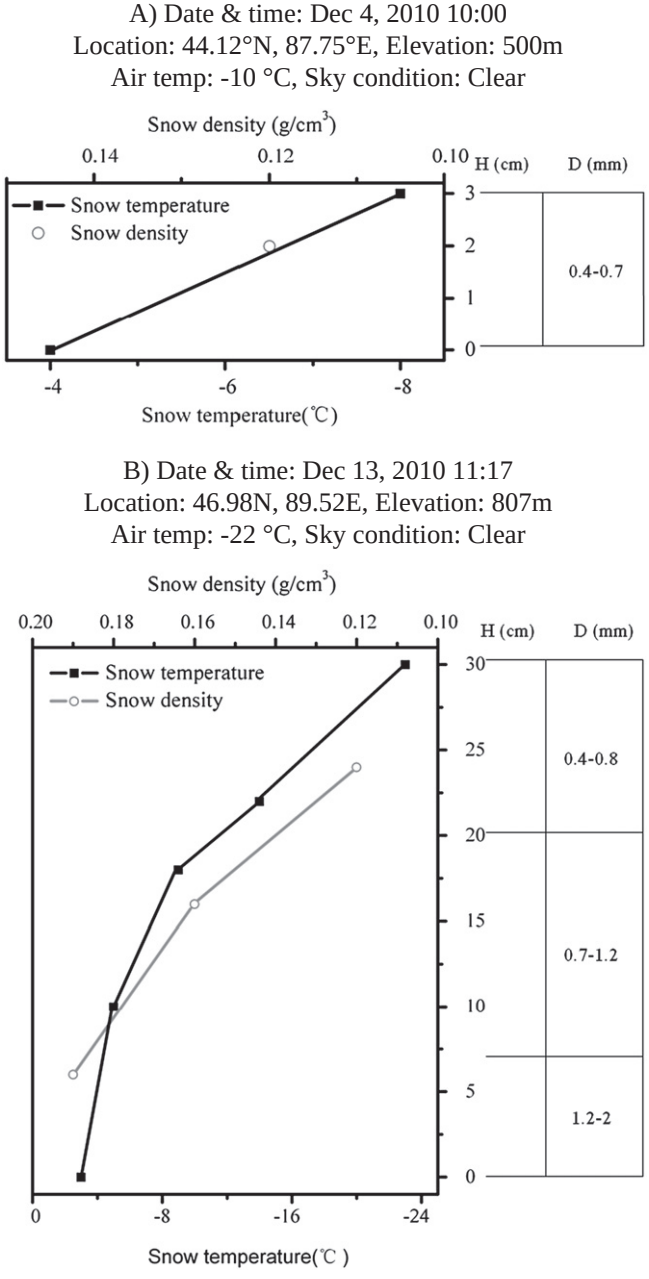

Fig. 2. Snow profile observed in Fukang (A), Fuyun (B), Cainan1 (C), Shixi (D) , Jichangcun (E) and Cainan2 (F). Black line: snow density; Gray line: snow temperature; D: Grain diameter; H: Height above snow-soil surface.

C) Date & time: Feb 25, 2011 16:00
Location: 44.99N, 88.469E, Elevation: 690m
Air temp: -13.4 °C, Sky condition: Clear

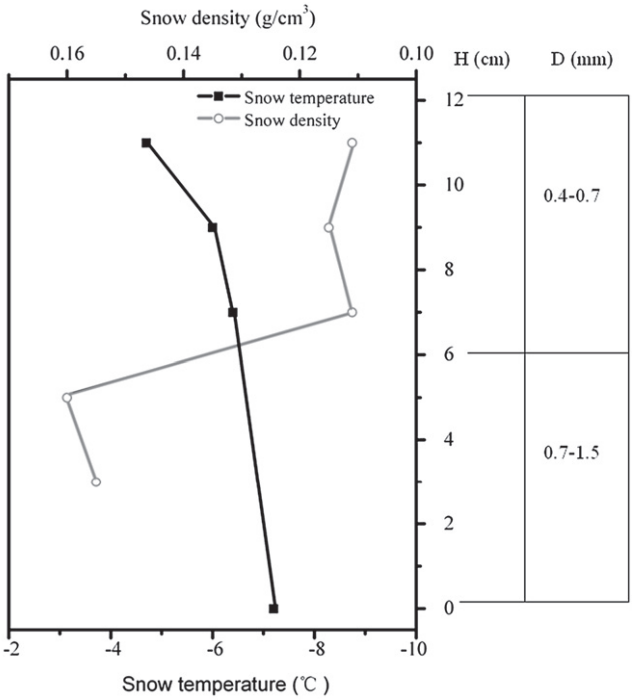

D) Date & time: Feb 26, 2011 12:00,
Location: 45.39N, 86.99E, Elevation: 426m
Air temp: -18.8 °C, Sky condition: Clear

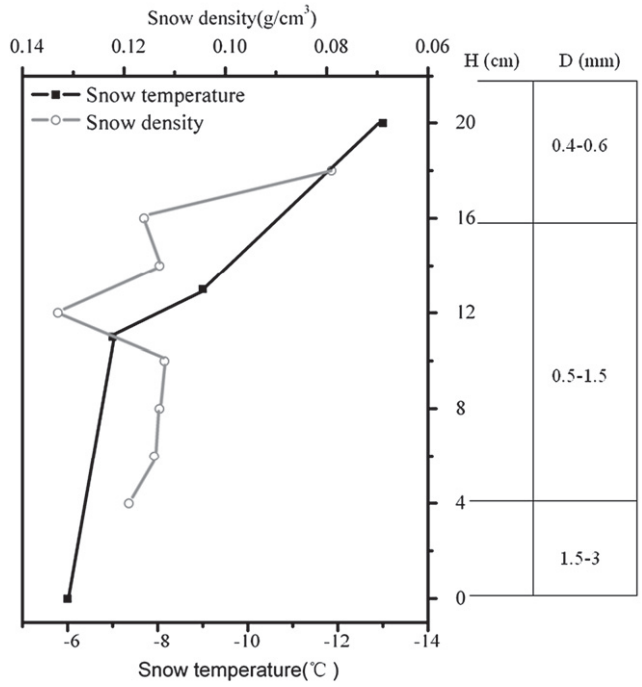

Fig. 2 (*continued*).

upper and bottom snow layer are generally less than that of the middle snow layer. For simplicity, we assume that the thickness of the upper snow layer is equal to the thickness of the bottom snow layer and half of the thickness of the middle snow layer. For the case of two snow layers, the same thickness is assumed for the upper and lower snow layers.

E) Date & time: Mar 1, 2011 12:50
Location: 47.75N, 88.061E, Elevation: 739m
Air temp: -16.7 °C, Sky condition: Clear

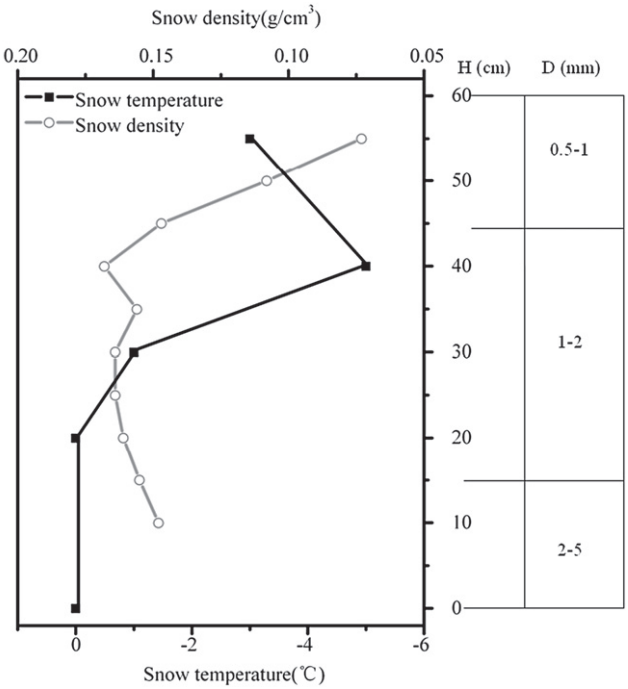

F) Date & time: Feb 27, 2011 12:00
Location: 44.99°N, 88.45°E, Elevation: 690m
Air temp: -16 °C, Sky con dition: Clear

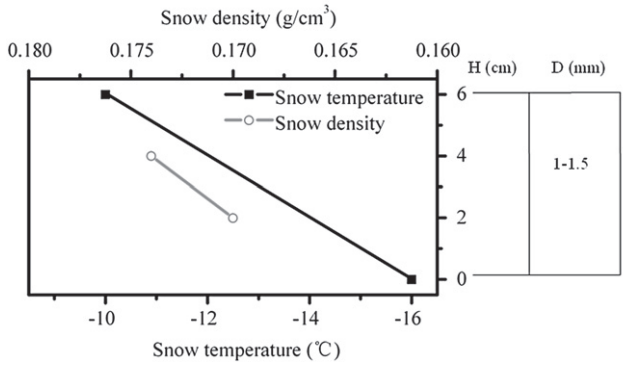

Fig. 2 (*continued*).

3.1.2. Snow density

Generally, for the vertical characterization of snow density, the upper layer of the snowpack is fresh snow, and its density is low, whereas the sub-layer snowpack is old snow and has undergone compaction and grain size growth; thus, its density is relatively higher according to the field measurements (Fig. 2). However, measurements from meteorological stations show that snow density increases smoothly from approximately 0.12 g/cm^3 to 0.22 g/cm^3 during the snow season (December 15 to March 20) but fluctuates at the beginning and the end of the snow season (Fig. 3). Therefore, a simple scheme is used to describe the dynamics of snow density with snow age for the three-layer case based on these observations (Table 2). For the case of two-layer snowpacks, only the upper and middle snow layers are retained; similarly, only the upper layer is retained for the one-layer case.

3.1.3. Correlation length

The correlation length is a parameter used for describing the influence of size and distribution of scatters (such as snow particle) on scattering, which is defined as the inverse of the derivative of autocorrelation function of snow structure at zero displacement. The snow structure can be described by a random two-valued function which is related to the volume fraction of ice in the background medium air (Wiesmann et al.,

Table 1
Statistics of snow grain size and snow density.

Snow type	New snow	Fine snow	Densified snow	Coarse grain	Depth hoar
Grain size (mm)	<0.5	0.5–1.0	1.0–2.0	2.0–3.0	>3.0
Density (g/cm^3)	0.11	0.17	0.22	0.24	0.25

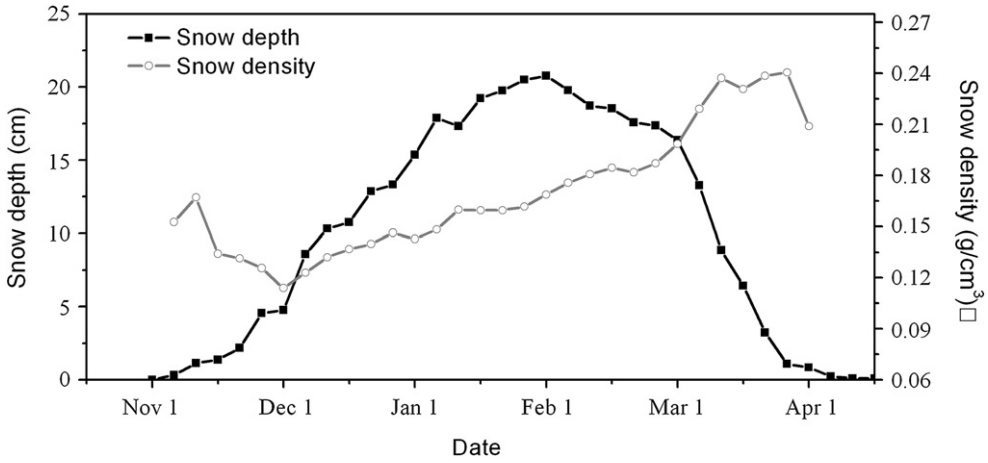

Fig. 3. Mean snow density and depth variation based on the measurements at thirteen meteorological stations during the snow season in Northern Xinjiang from 1999 to 2008.

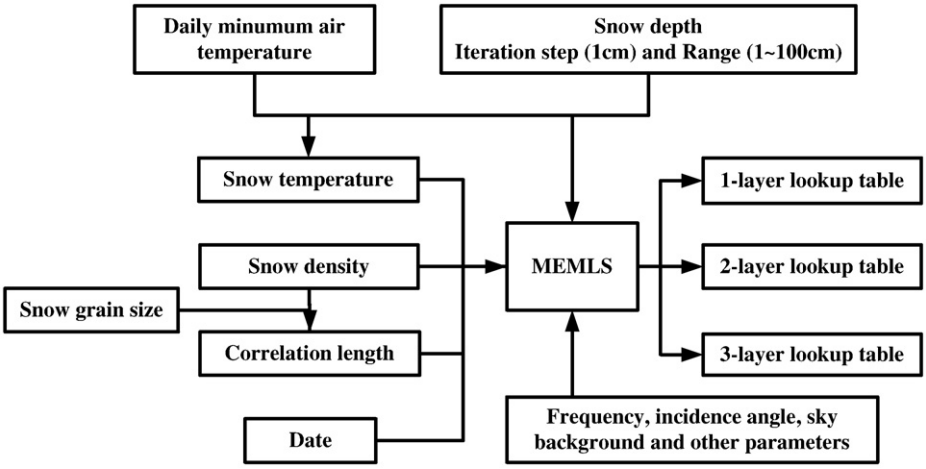

Fig. 4. Flow chart for the establishment of look-up tables.

1998). In this study, correlation length is used to describe the scattering of snow in the MEMLS model (Mätzler, 2002). According to Davis and Dozier (1989), the correlation length is related to snow grain size and density. Therefore, snow grain size and snow density should be determined first to infer the correlation length. Snow density was discussed in a previous section. Snow crystals in each layer of the snowpack include different dimensions; thus, we recorded the grain size in a range of diameters in the field measurements. Snow grain size has a similar vertical variation pattern to snow density and increases from the upper to lower layers. However, for the depth hoar case, snow grain size is extremely large, whereas snow density changes only slightly. In fact, snow grain size is related to snow density and snow age, and their general relationships are reported in Table 1.

Based on the field measurements, for the case of three-layer snowpacks, the variations of snow grain size with snow season are described in Table 3. For the case of two-layer and one-layer snowpacks, the upper layer is retained. For the two-layer case, snow grain size within the bottom layer is the weighted average of the values of the middle and bottom layer.

In this study, we used the method proposed by Davis and Dozier (1989) to convert grain size and density to the correlation length, and then converted the correlation length to exponential correlation

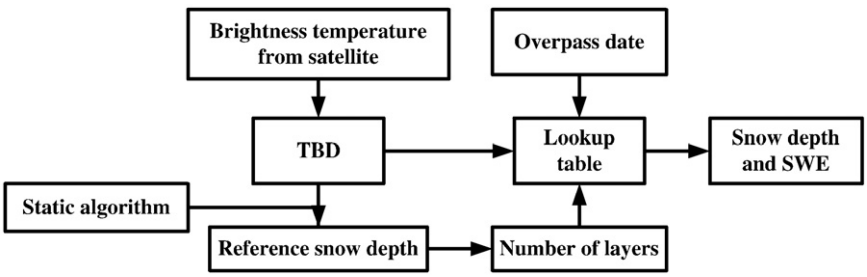

Fig. 5. Retrieval strategy of snow depth and SWE based on the look-up tables.

Table 2
Scheme of snow density (g/cm^3) dynamics with snow age.

	Upper layer	Middle layer	Bottom layer
Before December 15	0.11	0.15	0.2
February 1	0.11	0.16	0.215
March 1	0.13	0.195	0.235
April 1	0.17	0.235	0.27
After April 1	0.17	0.235	0.27

length by multiplying a constant (0.75) according to Mätzler (2002). For isotropic snow,

$$S = 2N \tag{3}$$

$$P_c = 4v(1-v)/S \tag{4}$$

$$P_c = \left(\rho/917 - \rho^2/917^2\right) \times D \tag{5}$$

$$P_{ex} = 0.75P_c \tag{6}$$

where S is the ice surface area per unit volume, v is volume fraction of ice, N is the intersect density which means the number of intersections per unit length of the ice-air surface, P_c is the correlation length, P_{ex} is the exponential correlation length, D is snow depth, and ρ is the snow density. According to the field measurements, the particle form is similar to the pillar, and the short-side length is between two-thirds and one times the long-side length. Given a uniform distribution of the snow grain size, 100 numbers were randomly generated according to the range of snow grain size, which represent the long-side length because the maximum diameter is often measured and recorded. For each of these 100 numbers, 100 numbers were randomly generated and the length range from two-thirds to the full length of the long-side length, which represents the length of the short-side. In total, we can obtain 10,000 snow crystals and assume that they are homogeneously distributed within a cubic box. Therefore, the volume of the cubic box can be calculated according to snow density and the volume of particles. N can be expressed by:

$$N = 2 \times a/n,$$

where a is the side length of the cubic box, and n is the particle number along its one side.

Based on formulae (3)–(6), the exponential correlation length can be calculated, and the typical results are presented in Table 4. These results agree well with the measurements of Wiesmann et al. (1998) and Mätzler (2002). Furthermore, the correlation length was calculated based on the snow grain size range and density for different layerings of snowpacks with snow age, which were previously determined (Fig. 6).

3.1.4. Snow temperature

For passive microwave remote sensing, snow temperature also influences the retrieval of snow depth to some extent. Kelly et al. (2003) assumed that the snow temperature is constant, but Tsutsui et al. (2007) assumed that it is equal to the ground temperature. In this study, the ground and snow temperatures were determined according to the relationship between the air temperature and snow depth.

Snow temperatures vary with time within one day; however, the temperature profiles in the observation snow pits described in Fig. 2 are measured during the daytime, which cannot reflect the actual snow temperature profiles at the AMSR-E overpass time. In this study, snow temperature profiles at sixteen snow pits were observed around the AMSR-E overpass time, and air temperature were also recorded (Table 5).

Air temperature is very close to its lowest value around this time, and there is a relationship between snow and air temperature for different snow depth. According to Table 5, when the snow depth is less than 30 cm, the difference between the air temperature and the temperature at the snow/soil interface increases linearly with the increase in snow depth, and the temperature at the air/snow interface is close to the air temperature (Fig. 7). In this study, it is assumed that the temperature on the air/snow interface is equal to the snow surface temperature. However, when the snow depth is greater than 30 cm, the temperature at the snow/soil interface remains approximately −2 °C, which may result from the thermal insulation of a deep snowpack. Therefore, the snow temperature (Ts) can be calculated from the daily minimal air temperature (Ta) and snow depth (SD):

$$\begin{aligned} Ts &= Ta + 0.71SD \quad \text{for } SD < 30 \text{ cm and} \\ Ts &= -2 \quad\quad\quad\quad\ \text{for } SD \geqq 30 \text{ cm}, \end{aligned}$$

where, unit of the Ts and Ta is °C, and unit of SD is cm.

3.1.5. Look-up tables

MEMLS was used to establish look-up tables for three cases of layering (one, two and three). Snow depth varies from 1 cm to 100 cm with an interval of 1 cm. The daily minimal air temperatures were obtained from meteorological stations, and the other variables and parameters have been discussed in the previous sections. Although the TBD at 18.7 GHz and 36.5 GHz was used to retrieve snow depth and SWE, the TBD at 10.7 GHz and 18.7 GHz was also accounted for in this study because the former cannot detect very deep snow cover (*i.e.*, the saturation phenomenon). When snow depth exceeds 60 cm, the TBD at 18.7 and 36.5 GHz tends to decrease (Tedesco and Narvekar, 2010). In this study, the snow grain size is large, and the brightness temperature at 36.5 GHz saturates at approximate 40 cm for a given grain size of deep snowpack, but the saturation point of brightness temperature at 10.7 GHz and 18.7 GHz is larger than the maximum snow depth in this study. Therefore, the TBD at 10.7 GHz and 18.7 GHz was adopted when snow depth is more than 40 cm. For convenience, the TBD at 18.7 GHz and 36.5 GHz will be noted by TBD1, and the TBD at 10.7 GHz and 18.7 GHz will be noted by TBD2 in the following context. Finally, three look-up tables corresponding to three types of layering can be obtained for each day of the snow season.

3.2. Retrieval scheme

According to this *a priori* information (snow layering, grain size, density, snow temperature and the temperature at the snow/soil interface), the MEMLS can simulate three look-up tables for each day.

Table 3
Scheme of snow grain size range (mm) dynamics with snow age.

	Upper layer	Middle layer	Bottom layer
Before December 15	0.4–0.7	0.5–1.2	1.0–2.0
February 1	0.4–0.7	0.7–1.5	1.5–2.5
March 1	0.5–1.1	1.0–2.0	2.0–3.0
April 1	0.7–1.5	1.5–3.0	3.0–4.0
After April 1	0.7–1.5	1.5–3.0	3.0–4.0

Table 4
Exponential correlation length (mm) in different grain sizes and snow densities.

Snow density (g/cm3)	Snow grain size (mm)				
	0.1–0.5	0.5–1	1–1.5	1.5–2	2–3
0.10	0.046	0.085	0.118	0.146	0.184
0.15	0.057	0.105	0.145	0.179	0.227
0.20	0.065	0.119	0.164	0.204	0.257
0.25	0.070	0.128	0.177	0.220	0.277
0.30	0.073	0.134	0.185	0.229	0.290

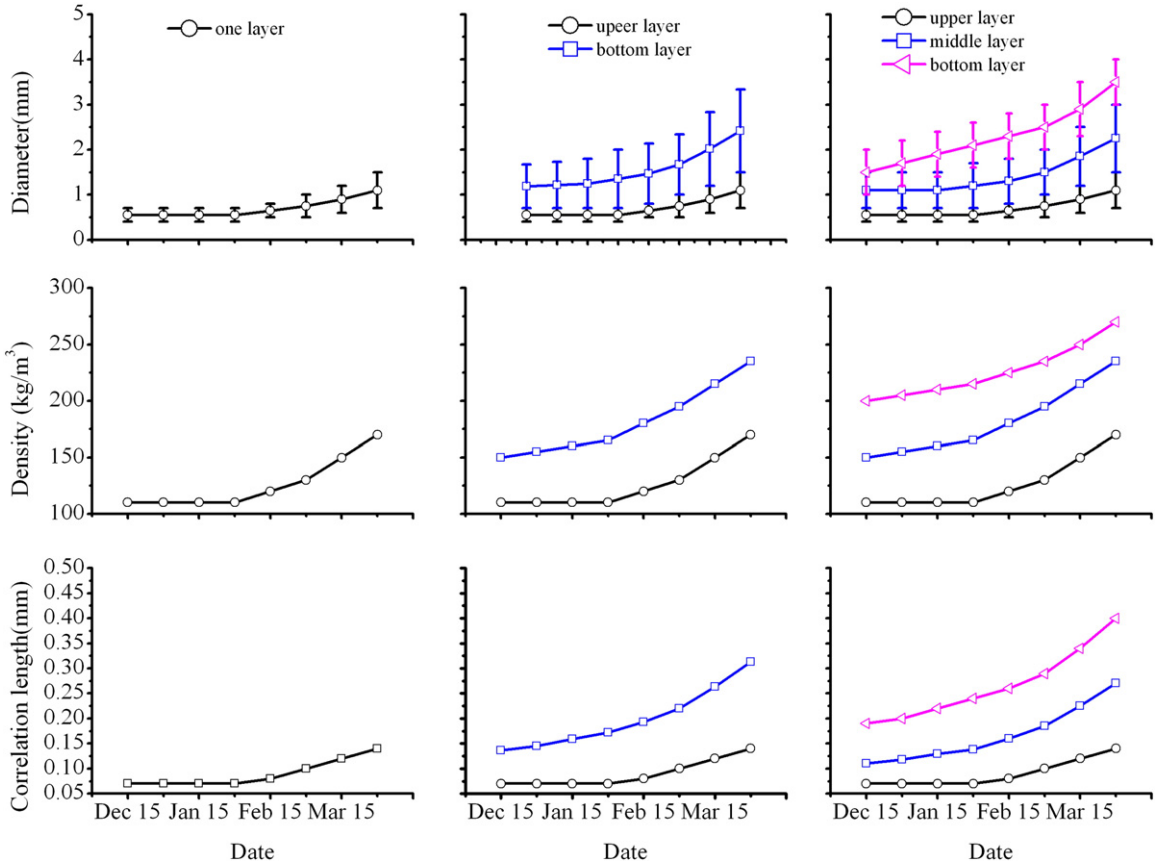

Fig. 6. Grain size, density and correlation length variations with snow age. Left: one-layer case, Middle: two-layer case, and Right: three-layer case.

These three look-up tables include TBD1 and TBD2 for all suitable snow properties, which are databases for snow depth and SWE retrieval by TBD1 and TBD2 that are calculated from AMSR-E data.

To retrieve snow depth and SWE based on these look-up tables, it is necessary to select an appropriate table, which includes two aspects: one aspect is the date of the satellite overpass, and the second aspect is the layering, which depends on the snow depth. For the second aspect, the TBD1 calculated from AMSR-E data is used to estimate an approximate snow depth and to determine the amount of layering based on the existing static snow depth retrieval algorithm (Che et al., 2008). In fact, there may be ambiguity when the snow depth is close to 10 cm or 20 cm due to uncertainties that result from the static

Table 5
Records of snow depth, soil-snow temperature and air temperature at 16 sample snow pits. Among these observations, the T_{snow} is the snow temperature close to soil except for the snow surface (0 cm) temperature measured at samples 1 and 2, and snow temperature at 2 cm from snow surface at sample 11.

Sample	Site	Local time	SD(cm)	Tair (°C)	Tsnow (°C)	Tsnow-Tair (°C)
1	44.12°N	2010.12.4 01:00	0	−11.5	−11	0.5
	87.75°E		5	−11	−7	4
2	(a)	2011.2.21 01:00	0	−20	−20	0
			7	−20	−12	8
3		2011.2.24 22:00	23	−25	−8	17
4		2011.2.24 22:10	17	−26	−12	14
5		2011.2.24 22:20	15	−26	−14	12
6	46.98°N	2010.12.15 23:00	33	−13	−2	11
7	89.52°E	2010.12.14 23:00	34	−16	−1.5	14.5
8	(b)	2010.12.13 23:00	29	−16.3	−2	14.3
9		2011.2.22 01:00	33	−20	−3.5	16.5
10		2011.2.22 01:00	32	−25	−2.5	22.5
11		2011.2.22 01:00	2	−23	−22.5	0.5
			30	−23	−2	21
12	45.38°N	2011.2.26 07:00	21	−23	−8.3	14.7
13	86.99°E	2011.2.26 07:10	20	−23	−8.5	14.5
14	(d)	2011.2.25 22:00	14	−19	−9	10
15		2011.2.25 22:13	11	−19	−12	7
16	47.75°N	2011.3.1 07:30	60	−20	−1	19
	88.06°E					
	(e)					

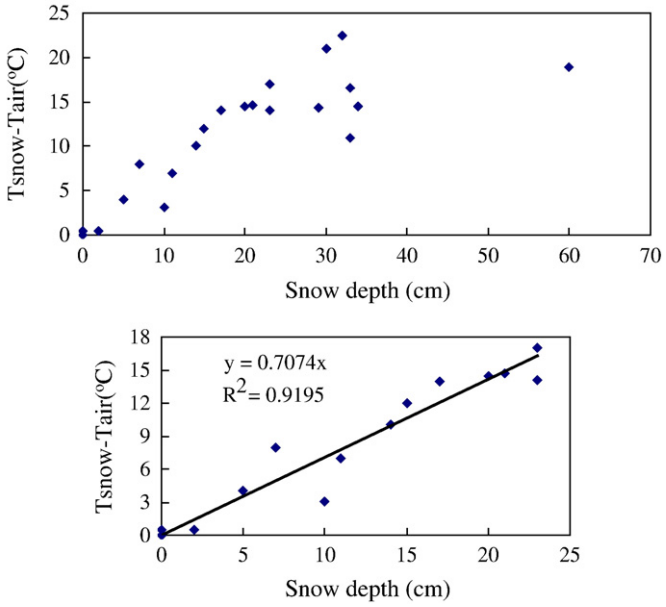

Fig. 7. Relationship between snow depth and temperature differences between air temperature and soil-snow interface temperature for all study samples (above) and for samples in which snow depth was less than 30 cm (below).

retrieval algorithm; therefore, two snow depth transitional zones are accounted for, and the criteria are:

TBD1 <= 7 K	for one−layer,
7 k < TBD1 <= 12 K	for one−layer and two−layer,
12 k < TBD1 <= 20 K	for two−layer,
20 k < TBD1 <= 25 K	for two−layer and three−layer, and
TBD1 > 25 K	for three−layer.

The amount of snow layering and the look-up table will be determined, and the TBD1 will correspond to unique snow properties. Snow depth and density can be found using TBD1 that is calculated using the AMSR-E data at 18 GHz and 36 GHz, and SWE can be obtained by the snow depth and density. However, TBD1 may not increase with snow depth when snow grain size and snow depth are very large according to the simulations of the MEMLS, which is a type of microwave saturation phenomenon (Tedesco and Narvekar, 2010; Vachon et al., 2010). For this case, TBD2 can describe the snow properties because of their longer wavelengths, which indicates greater penetration depth and insensitivity to snow grain size (Tedesco and Narvekar, 2010). Therefore, TBD2 will be used to find the optimal snow depth and SWE when TBD1 is higher than 40 K.

4. Uncertainties

The look-up table uncertainties included two aspects; one aspect is the MEMLS, which is used to simulate the brightness temperature, and the other aspect is the inputs of the *a priori* information. The MEMLS that is used to establish the look-up tables was developed based on snow measurements to determine the relationships between the snow's physical properties and microwave properties. The accuracy of the MEMLS is discussed by Wiesmann and Mätzler (Mätzler and Wiesmann, 1999; Tedesco and Kim, 2006; Wiesmann and Mätzler, 1999). The uncertainties from the *a priori* information are discussed here, which include the layering scheme of the snowpack, the snow temperature, the emissivity of the underlying ground and wet snow.

4.1. Layering scheme

In this study, snow cover is divided into one, two, or three layers according to snow depth, which is estimated from TBD, and two transitional zones are proposed to remove the ambiguities of the number of layers. The proportion of each layer is fixed once the number of layers is determined, namely, the thickness of the upper and bottom

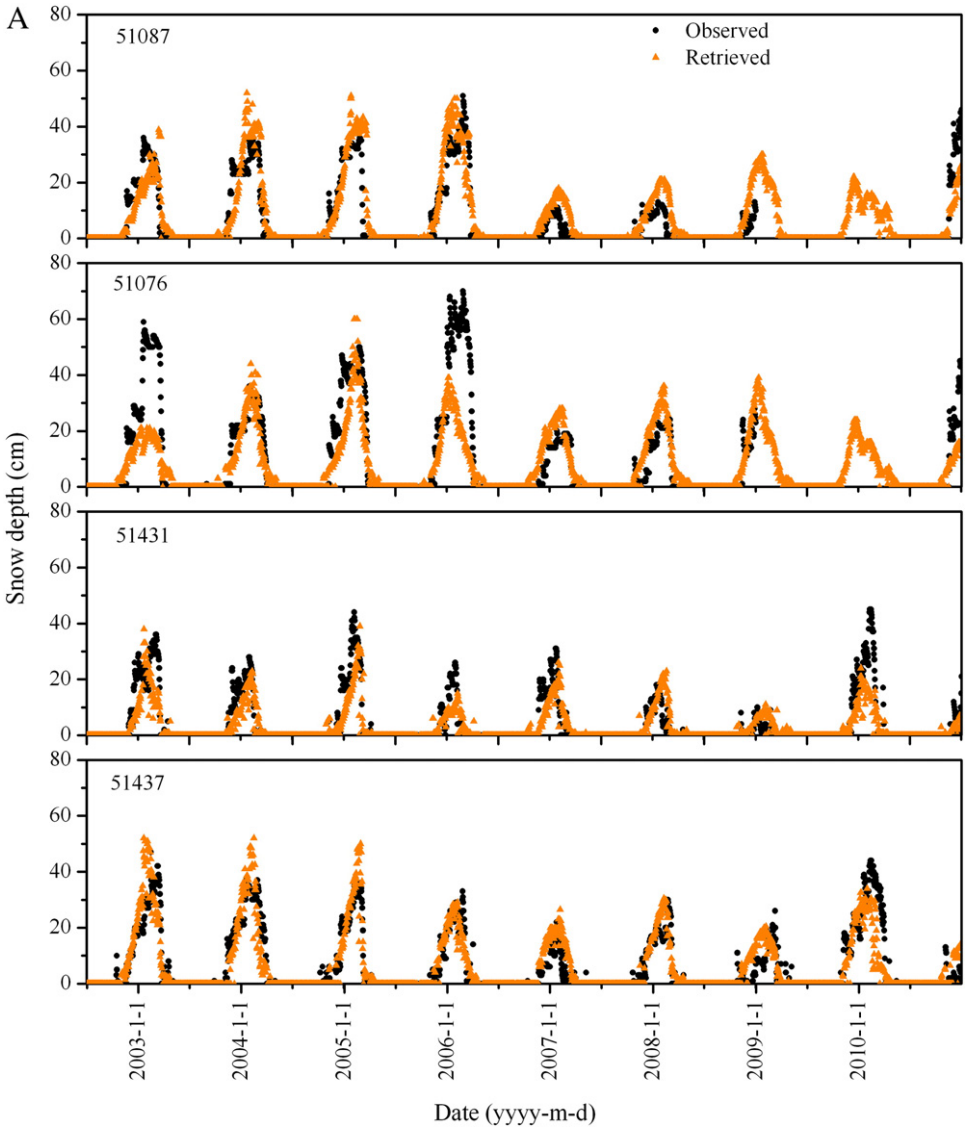

Fig. 8. Comparisons of snow depth estimated from the new algorithm and observed from station for 13 stations ((A) for deep snow, (B) for moderate snow, (C) for shallow snow). Note: In the graph of station 51068 of (B), the blue points "retrieved (2)" is the snow depth retrieved at the AMSR-E grid over station 51068, while the orange points "retrieved" is the snow depth retrieved at the east grid of the AMSR-E grid over station 51068.

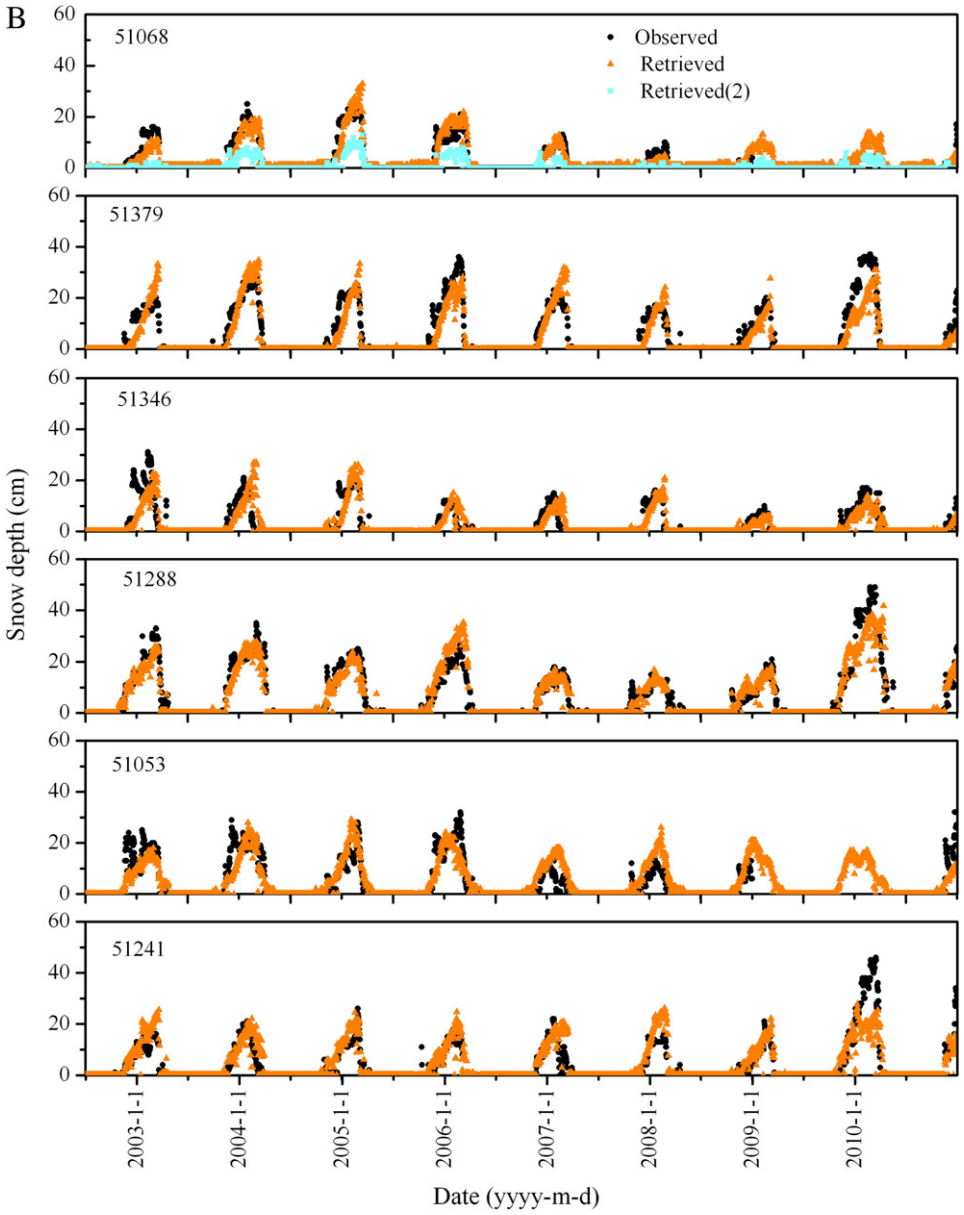

Fig. 8 (*continued*).

layers is equal for the case of two layers, and a middle layer with a half of a snowpack is added into the upper and bottom layers (these two layers have same thickness) for the case of three layers. This layering scheme corresponds to most of the field measurements, although it will be less reliable when heavy snowfall occurs. Therefore, a large mass of new snow will create a deeper upper layer and a smaller snow grain size and density, which can lead to underestimation of snow depth when this method is used. Furthermore, there may be an ice layer within the snowpack because of refreezing, which can make the snow layering more complicated (Durand et al., 2008). However, these problems are not considered by this empirical look-up table method, which is suitable only for general snow conditions.

4.2. Snow temperature

The contributions of snow temperature at the different depths of the snowpack (in the vertical direction) to brightness temperature are different for microwave frequencies. In this study, the layered snow temperature is determined using the linear relationship between the difference between temperature at the snow/soil interface and the air temperature and snow depth. However, the increase in the temperature at the snow/soil interface to the underlying ground may not be linear, which can result in temperature uncertainties at some snow layers. The actual snow temperature profiles in different snow conditions are also quite different (Vachon et al., 2010). Therefore, we analyzed the uncertainty of snow temperature based on the MEMLS. Given that the snow depth is 30 cm, the correlation length is 0.2 mm, and the underlying ground temperature is 270 K, the difference of TBDs between a maximum 270 K and a minimum 250 K of snow temperature is less than 5 K based on the simulation of the MEMLS. However, the error in snow temperature from the empirical formula (in Section 3.1.4) used in this study is less than 5 K, which can lead to an error of approximately 1.2 K for TBD and of approximately 1 cm for snow depth.

4.3. Emissivity of the underlying ground

The ground covered by snow is assumed to be frozen soil, and its emissivity is set as 0.93 for all microwave frequencies. However, the

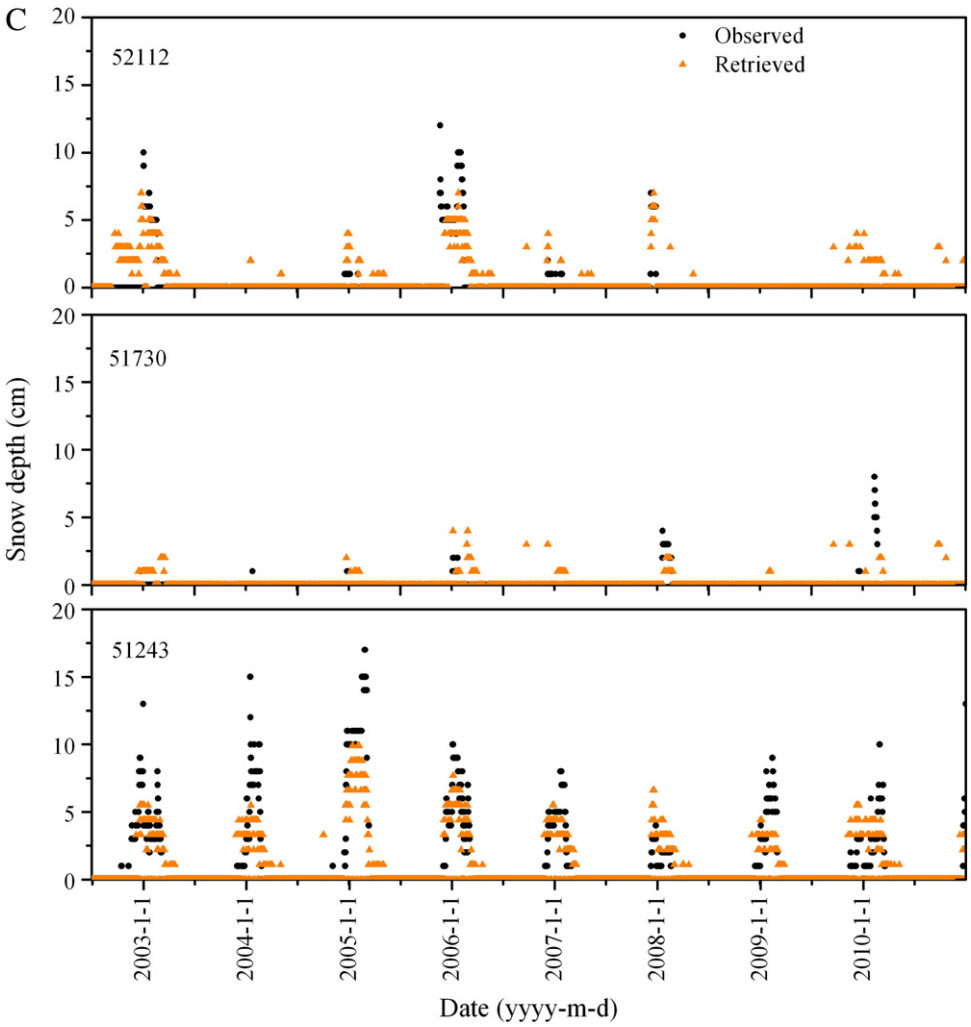

Fig. 8 (*continued*).

emissivity at 18 GHz and 36 GHz is different and depends on the ice content and soil texture (Grody and Basist, 1996; Jin et al., 2009). This difference can be ignored for deep snow but has an influence on the estimation of snow depth when snow is shallow because of the weak attenuation of microwave radiation from the ground. At present, there are not enough data to analyze the ground emissivity in this study. However, a coupled microwave radiative transfer model designed to describe the microwave properties of frozen soil covered by snow could be developed to resolve this problem.

4.4. Wet snow

When snow is wet, snow depth can't be retrieved by passive microwave remote sensing data (Tedesco and Narvekar, 2010). According to our field measurements in this region, the liquid water can be found at a very thin layer (1 cm) at the surface of snow cover around noon time. In this study, the air temperature from the meteorological stations was very low from October to April, and the daily lowest temperature was lower than −7 °C before snow disappearance. On the other hand, we used the criteria in Tedesco and Narvekar (2010) to identify the wet snow. When the brightness temperatures at 36 GHz of horizontal is more than 245 K or that at 36 GHz of vertical polarization is more than 255 K, all observed snow depth is zero. Therefore, there was not wet snow cover during the study period. Anyway, it is necessary to make sure if there is wet snow cover before the method in this study is used in other regions.

5. Results and validations

In sum, AMSR-E data from approximately eight years were collected to retrieve the snow depth and SWE (determined by snow depth and density) in Xinjiang using these look-up tables. To validate these results, the snow depth and SWE retrieved from AMSR-E brightness temperatures based on the proposed method are compared with the following data: 1) snow depth data from July 1, 2002 to December 31, 2010 from thirteen meteorological stations in the study area; 2) Northern hemisphere SWE product from the European Space Agency (ESA), global AMSR-E SWE products obtained from the National Snow and Ice Data Center (NSIDC) and snow depth derived from passive microwave remote sensing data in China obtained from Environmental and Ecological Science Data Center for West China (WESTDC) (Che et al., 2008; Li et al., 2011); and 3) snow depth measurements along the snow course during the field experiment in February 2011.

5.1. Comparisons with snow depths of meteorological stations

The thirteen meteorological stations are divided into three groups according to averaged snow depth, namely, deep snow, medium

snow and shallow snow (Fig. 8). Good agreement in snow depth can be found for all three groups between the station observations and the retrieved results. The estimations and observations have good agreement for snow accumulation and ablation periods throughout the snow season, and the root mean squared error (RMSE) and bias during the snow season are 11.2 and −2.8 cm for the deep snow group, 6.3 and −0.7 cm for the medium deep snow group, and 2.1 and −0.9 cm for the shallow snow group (Table 6).

However, large errors were identified in several years, such as in the results from Station 51076 in 2003 and 2006, Station 51431 in 2010, and Station 51241 in 2010. When large errors occur, snow depths rapidly increase (up to 30 cm for 51076 and 51431, 20 cm for 51241) within five days, suggesting that there are continuous and heavy snowfall events, leading to greater thickness featured with small snow grain size (fresh snow). The method proposed in this study uses the snow grain size as the main factor to determine the layer of snowpack, and the layering scheme cannot reflect this type of rare phenomenon. In this case, the real snow grain size is overestimated; therefore, the snow depth is underestimated because a shallower snowpack with large grain size also exhibits strong volume scattering.

A special case should be mentioned here; Station 51068 is located on the west side of a lake. The snow depth is obviously underestimated from the AMSR-E grid data over this station (the points "retrieved (2)" in Fig. 8B); however, the snow depth from the AMSR-E data of its neighboring grid was in good agreement with the observations from the station (Fig. 8B). It is obvious that the frozen water body has an influence on snow depth retrieval, which was noted by Dong et al. (2005). Although the lake is small and frozen, its influence cannot be ignored. At this point, our results are slightly different from the findings of Dong et al. (2005). The lake has an influence on the retrieval of snow depth within the passive microwave remote sensing pixel but not the neighbor pixel. Therefore, a microwave radiative transfer model that includes lake ice may improve the retrieval of snow depth (Derksen et al., 2009; Lemmetyinen et al., 2011) in this area and others like it.

Table 6
Mean and maximum snow depth of measurements at meteorological stations and errors of snow depth estimated from the new algorithm compared to snow depth measured at thirteen stations in Xinjiang, China from 2003 to 2008. These statistics are divided into three groups based on the mean snow depths of the station measurements (a) For all data and (b) for the snow season only.

Station ID	Mean snow depth (cm)	Maximum snow depth (cm)	Bias (cm)	RMSE (cm)	Correlation
(a)					
Deep snow					
51087	6.4	49	1.8	6.9	0.86
51076	9.7	67	−0.4	10.6	0.78
51431	3.8	44	−0.9	5.6	0.76
51437	6.2	69	−0.9	7.3	0.85
Mean	6.5	57.3	−0.1	7.6	0.81
Medium snow					
51241	4.0	26	0.4	4.2	0.88
51053	4.8	29	0.4	3.8	0.81
51288	6.5	33	−0.1	7.0	0.78
51346	2.7	30	−0.3	3.3	0.76
51379	5.2	36	−0.9	3.5	0.92
51068	3.1	23	0.3	2.1	0.89
Mean	4.4	29.5	0.0	4.0	0.84
Shallow snow					
52112	0.3	10	0.1	1.0	0.63
51730	0.1	3	0.0	0.5	0.32
51243	1.1	13	−0.3	1.7	0.78
Mean	0.5	8.7	−0.1	1.1	0.58
(b)					
Deep snow					
51087	18.6	49	2.3	10.0	0.67
51076	26.4	67	−7.2	17.1	0.38
51431	16.8	44	−5.4	8.0	0.47
51437	18.6	69	0.6	9.5	0.62
Mean	20.1	57.3	−2.8	11.2	0.54
Medium snow					
51241	12.3	26	0.9	7.0	0.61
51053	13.0	29	−0.1	7.2	0.37
51288	16.45	33	−0.2	5.7	0.80
51346	10.2	30	−1.5	6.3	0.50
51379	16.8	36	−2.6	6.9	0.72
51068	10.3	23	−0.7	4.5	0.79
Mean	13.2	29.5	−0.7	6.3	0.63
Shallow snow					
52112	5.3	10	−1.0	2.3	0.50
51730	2.4	3	−0.9	1.3	0.09
51243	5.1	13	−0.8	2.8	0.65
Mean	4.3	8.7	−0.9	2.1	0.41

5.2. Comparisons with products from NSIDC, ESA and WESTDC

AMSR-E/Aqua Daily L3 Global Snow Water Equivalent EASE-Grids are available from the NSIDC. This product is generated from the AMSR-E/Aqua L2A Global Swath Spatially Resampled Brightness Temperature unresampled data. The probability of snow per pixel is determined using snow cover maps from Dewey and Heim (1981) and the land/ocean/ice mask. The brightness temperatures for different channels are checked to determine if snow is likely to be shallow or medium-to-deep (Foster et al., 2011). If snow presence is detected but is likely to be shallow, the snow depth is estimated as 5.0 cm. For medium-to-deep snow, separate retrievals for forested and un-forested fractions are combined to obtain the entire snow depth within the AMSR-E pixel. A detailed algorithm is given by (Kelly, 2009; Tedesco and Narvekar, 2010). SWE is estimated using the snow depth and the ancillary snow density data (SWE = SD (cm) * density (g/cm^3) * 10.0 (mm)).

ESA GlobSnow SWE dataset was produced by the algorithm that assimilated synoptic weather station snow depth observations with satellite passive microwave brightness temperature (Takala et al., 2011). The basis of this algorithm was presented in an article by Pulliainen (2006), and the effective value of snow grain size was optimized by HUT (Helsinki University of Technology) snow emission model with snow depth observed from stations and satellite brightness temperature. Furthermore, these values of grain size were interpolated by the Kriging technique to obtain the background map of the effective grain size. The snow density was treated with a constant value of 0.24 g/cm^3. A map of spatially continuous 'assimilated SWE' was produced through forward brightness temperature simulations with the HUT model using the interpolated effective grain size and land cover information (Takala et al., 2011).

The snow depth product for China is available from the WESTDC. This product is derived from the AMSR-E/Aqua EASE-Grid temperature using the algorithm proposed by (Che et al., 2008). This algorithm modified the coefficient of the Chang algorithm (Chang et al., 1976) using snow depth observations from meteorological stations in China and used an average offset to remove the influence of snow density and grain size seasonal variations with a simple statistical method.

These three snow products are compared with the SWE from the new algorithm. The observations from the meteorological stations are used as references. NSIDC and ESA provide SWE products, and WESTDC provides snow depth products. Therefore, snow density measured at the meteorological stations, which can be calculated from snow pressure and snow depth by formula 2, is used to convert snow depth to SWE. However, the snow pressure is measured only when the snow depth is greater than 5 cm at these stations; thus, medium-to-deep snow data are selected to compare these results in this study.

By comparing the snow water equivalent measured from the stations, the mean RMSEs of methods from this study, WESTDC, ESA and NSIDC, were found to be 14.6 mm, 18.4 mm, 23.8 mm and 75.8 mm, respectively, for the deep snow group and 8.9 mm, 12.9 mm, 26.8 mm and 41.3 mm, respectively, for the medium

snow group. The mean biases of the methods from this study, WESTDC, ESA and NSIDC, are −0.9 mm, 0.0 mm, 17.8 mm and 63.6 mm, respectively, for the deep snow group and −1.6 mm, −2.8 mm, 17 mm and 26.6 mm, respectively, for medium snow group (Table 7). NSIDC products show the largest errors for RMSE and bias, which may be because the information of snow grain size and snow density within the global SWE algorithm are not suitable for snow properties in this study area (Foster et al., 1997). The products from ESA show much more accurate than that from NSIDC, because the ESA algorithm assimilates synoptic weather station snow depth observations. The WESTDC method used snow depth observations on meteorological stations in China to modify the snow depth global algorithm; therefore, its result is close to the observations on these stations. The new algorithm in this study considers the local snow properties in detail and shows the best agreement with the meteorological station observations.

5.3. Comparisons with snow depth along a snow course

From February 25 to March 2, 2011, we measured the snow course around the Junggar Basin, and no snowfall during this period was detected; the route is shown in Fig. 1, and the exact measurement points are shown in Fig. 9a. The measured snow depths were compared with the estimated snow depth in Xinjiang, China on February 26, 2011, and they matched well (Fig. 9b). The bias was 2.6 cm, the RMSE was 7.3 cm, and the correlation coefficient was 0.8 (correlation is significant at the 0.01 level). Several large errors were found at the most northern course, where very deep snow was observed during the field experiment; however, this is a transitional zone of very shallow snow and very deep snow cover with a direction from southwest to northeast. The passive microwave remote sensing has a coarse footprint, which results in a smooth estimation of snow depth by the AMSR-E.

Table 7
The mean SWE of measurements at the meteorological stations and errors of SWE estimated from the new algorithm, and the SWE products from WESTDC and NSIDC compared to SWE measured at ten stations in Xinjiang from 2003 to 2008. These statistics are divided into two groups based on the mean snow depth of station measurements (a) For all data and (b) for the snow season only.

Station ID	Mean SWE (mm)	Bias(mm)				RMSE(mm)			
		New	WESTDC	ESA	NSIDC	New	WESTDC	ESA	NSIDC
(a)									
Deep snow									
51087	9.7	3.6	1.9	9.2	48.1	10.6	9.1	18.4	83.9
51706	16.9	−0.9	−4.3	5.8	49.7	16.2	18.7	14.7	71.7
51431	6.8	0.2	−1.1	4.1	15.9	7.1	9.8	11.9	34.8
51437	9.1	1.2	0.9	1.7	28.3	6.3	8.9	12.6	48.7
Mean	10.6	1.0	−0.7	5.2	35.5	10.1	11.6	14.4	59.8
Medium snow									
51241	8.1	4.2	−0.1	6.4	19.0	17.5	12.5	16.1	42.3
51053	4.4	0.1	0.2	7.3	7.7	3.8	6.5	20.9	15.1
51288	9.2	−3.0	−5.3	4.6	7.7	10.4	31.9	11.7	39.1
51346	3.5	0.6	−0.1	5.6	5.1	5.8	47.0	14.4	50.1
51379	9.1	0.8	−2.8	1.3	22.2	7.7	9.5	8.6	54.3
51068	5.4	−2.4	−3.2	6.7	8.4	6.5	5.1	17.6	30.8
Mean	6.6	0.1	−1.9	5.3	11.7	8.6	18.8	14.9	38.6
(b)									
Deep snow									
51087	33.4	0.5	7.4	25.6	84.6	14.8	15.0	30.1	105.1
51706	49.5	−2.4	−12.0	17.1	70.6	20.6	23.8	26.4	85.4
51431	30.5	−3.1	−2.8	17.9	38.0	13.8	19.6	20.7	38.8
51437	33.8	1.3	7.4	10.7	61.1	9.0	15.1	18.1	74.0
Mean	36.8	−0.9	0.0	17.8	63.6	14.6	18.4	23.8	75.8
Medium snow									
51241	18.8	−2.0	−1.9	20.8	12.4	5.3	10.0	29.4	18.8
51053	25.7	−3.6	−5.7	21.8	−6.4	11.6	13.9	36.8	16.7
51288	24.6	3.5	4.2	10.7	20.1	10.5	15.6	18.1	16.3
51346	16.4	−0.4	−4.7	20.75	37.8	6.4	8.4	27.8	54.0
51379	28.6	−3	−3.9	4.3	73.5	10.3	13.7	15.8	99.4
51068	22.4	−4.3	−4.8	23.5	21.9	9.2	15.9	33	42.7
Mean	22.8	−1.6	−2.8	17.0	26.6	8.9	12.9	26.8	41.3

6. Conclusion

In this study, a novel algorithm was developed to retrieve snow depth/SWE in Xinjiang, China based on a look-up table method that was proposed by Tedesco and Narvekar (2010). Within this algorithm, the snow stratigraphy and its grain size, density, and temperate variations spatiotemporally within a snow season are determined *a priori* and are based on field experiments.

The estimations of snow depth and SWE from AMSR-E data from 2002 to 2010 show good consistency with the observations at thirteen meteorological stations. The RMSE and bias during the snow season were 11.2 and −2.8 cm, respectively, for deep snow stations, 6.3 and −0.7 cm, respectively, for the medium-deep snow group, and 2.1 and −0.9 cm, respectively, for the shallow snow group. There was good consistency among the snow depth measurements along the snow course with a bias of 2.6 cm and an RMSR of 7.3 cm.

Compared to the existing snow depth and SWE products, the snow depth/ SWE in this study is a slight improvement over the snow depth data from WESTDC, moderately improvement over the SWE data from ESA and an obvious improvement over the SWE data from NSIDC were found based on the measurements at the meteorological stations. Compared to the snow water equivalent that was measured from the stations, the mean RMSEs of the methods from this study, WESTDC, ESA and NSIDC, are 14.6 mm, 18.4 mm, 23.8 mm and 75.8 mm, respectively, for the deep snow group, and 8.9 mm, 12.9 mm, 26.8 mm and 41.3 mm, respectively, for the medium snow group. The mean biases of the methods from this study, WESTDC and NSIDC, are −0.9 mm, 0.0 mm, 17.8 mm and 63.6 mm, respectively, for the deep snow group and −1.6 mm, −2.8 mm, 17.0 mm and 26.6 mm, respectively, for the medium snow group.

According to the snow depth measurements at the meteorological stations in China, the algorithm of snow depth from WESTDC was developed by modifying the coefficient of the global algorithm of snow depth (Chang et al., 1987) and removing the seasonal bias by an empirical offset (Che et al., 2008). Therefore, it is not surprising that the snow depth product from WESTDC is closer to the measurements at the meteorological stations than the snow product from ESA and NSIDC. The ESA algorithm assimilates the synoptic weather station snow depth observations, so it is much more accurate than the NSIDC algorithm.

However, the look-up tables used in this study, which adopt more snow characteristics as *a priori* information (in particular, the snow grain size and density), showed a better estimation of snow depth. Therefore, it is important to know the local snow properties and their seasonal variations for accurate retrievals of snow depth and SWE from passive microwave remote sensing. This method can also be applied to other passive microwave brightness temperature data, such as SMMR (Scanning Multichannel Microwave Radiometer), SSM/I (Special Sensor Microwave Imager) and FY-3 MWRI (Microwave Radiometer Imager boarded on FY-3 satellite), to obtain snow depth and SWE data in Xinjiang, China.

Acknowledgment

The availability of the snow data provided by the centre for Meteorological Information Services, China Meteorological Administration is appreciated. The authors thank Xinjiang Institute of Ecology and Geography, Chinese Academy of Sciences for providing logistics during the field work. This study is supported by the China State Key Basic Research Project (2010CB951403), and the Chinese National Natural Science Foundation (40971188 and 40601065).

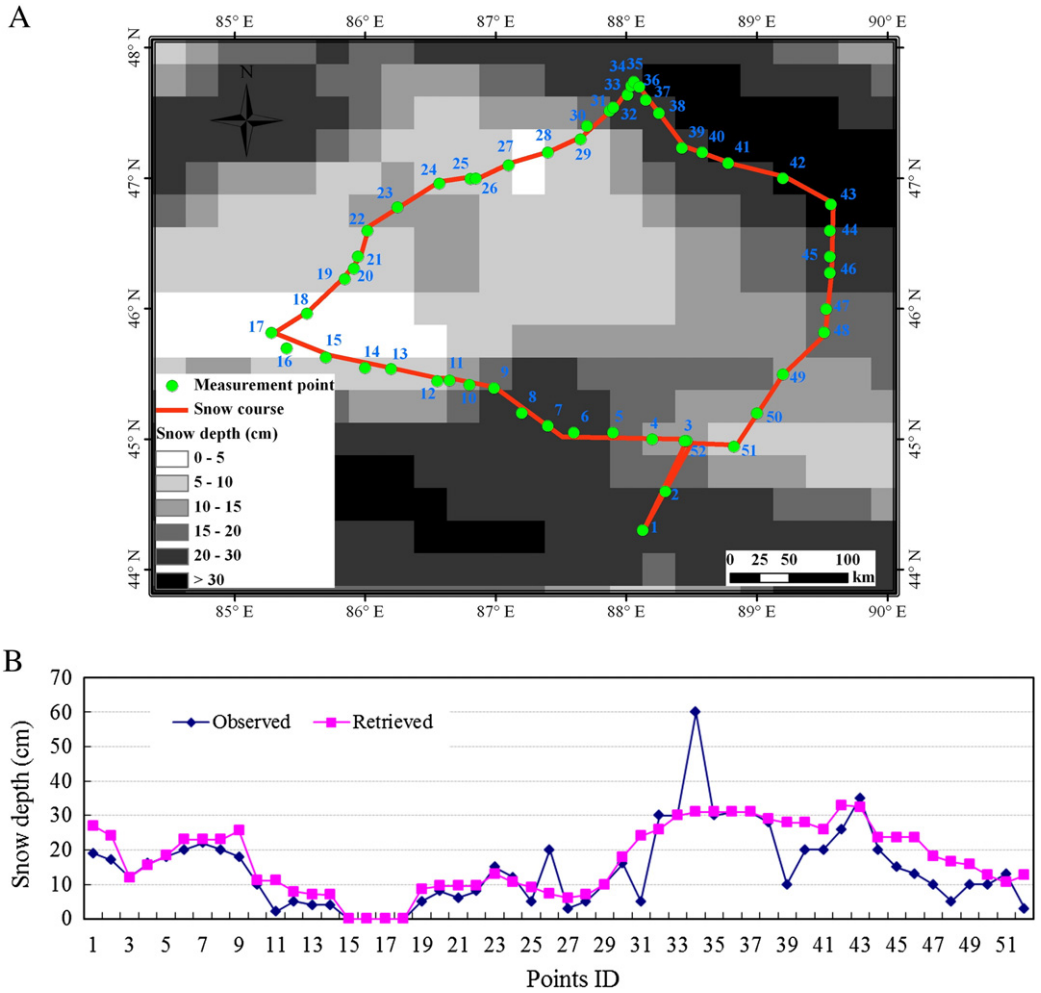

Fig. 9. (A) Route and measurements point locations of snow course and (B) comparisons of snow depth between snow course and retrievals.

References

Chang, A. T. C., Foster, J. L., & Hall, D. K. (1987). Nimbus-7 SMMR derived global snow cover parameters. *Annals of Glaciology*, *9*, 39–44.

Chang, A. T. C., Gloersen, P., Schmugge, T., Wilheit, T. T., & Zwally, H. J. (1976). Microwave emission from snow and glacier ice. *Journal of Glaciology*, *16*, 23–39.

Che, T., Dai, L. Y., Wang, J., Zhao, K., & Liu, Q. (2011). Estimation of snow depth and snow water equivalent distribution using airborne microwave radiometry in the Binggou Watershed, the upper reaches of the Heihe River Basin. *International Journal of Applied Earth Observation and Geoinformation*. http://dx.doi.org/10.1016/j.jag.2011.10.014.

Che, T., Li, X., Jin, R., Armstrong, R., & Zhang, T. J. (2008). Snow depth derived from passive microwave remote-sensing data in China. *Annals of Glaciology*, *49*, 145–154.

Davis, R. E., & Dozier, J. (1989). Stereological characterization of dry alpine snow for microwave remote sensing. *Advances in Space Research*, *9*(1), 245–251.

Derksen, C., Sturm, M., Liston, G. E., Holmgren, J., Huntington, H., Silis, A., et al. (2009). Northwest territories and Nunavut snow characteristics from a subarctic traverse: Implications for passive microwave remote sensing. *Journal of Hydrometeorology*, *10*, 448–463.

Derksen, C., Toose, P., Rees, A., Wang, L., English, M., Walker, A., et al. (2010). Development of a tundra-specific snow water equivalent retrieval algorithm for satellite passive microwave data. *Remote Sensing of Environment*, *114*, 1699–1709.

Dewey, K. F., & Heim, R. Jr (1981). Satellite observations of variations in northern hemisphere seasonal snow cover. *NOAA Technical Report NESS*, *87*.

Dong, J. R., Walker, J. P., & Houser, P. R. (2005). Factors affecting remotely sensed snow water equivalent uncertainty. *Remote Sensing of Environment*, *97*, 68–82.

Dressler, K. A., Leavesley, G. H., Bales, R. C., & Fassnacht, S. R. (2006). Evaluation of gridded snow water equivalent and satellite snow cover products for mountain basins in a hydrologic model. *Hydrological Processes*, *20*, 673–688.

Durand, M., Kim, E. J., & Margulis, S. A. (2008). Quantifying uncertainty in modeling snow microwave radiance for a mountain snowpack at the point-scale, including stratigraphic effects. *IEEE Transaction on Geoscience and Remote Sensing*, *46*(6), 1753–1767.

Foster, J. L., Chang, A. T. C., & Hall, D. K. (1997). Comparison of snow mass estimates from prototype passive microwave snow algorithm, a revised algorithm and a snow depth climatology. *Remote Sensing of Environment*, *62*(2), 132–142.

Foster, J. L., Hall, D. K., Eylander, J. B., Riggs, G. A., Nghiem, S. V., Tedesco, M., et al. (2011). A blended global snow product using visible, passive microwave and scatterometer satellite data. *International Journal of Remote Sensing*, *32*(5), 1371–1395.

Foster, J. L., Hall, D. K., Kelly, R. E. J., & Chiu, L. (2009). Seasonal snow extent and snow mass in South America using SMMR and SSM/I passive microwave data (1979–2006). *Remote Sensing of Environment*, *113*, 291–305.

Foster, J. L., Sun, C., Walker, J. P., Kelly, R., Chang, A. C. T., Dong, J. R., et al. (2005). Quantifying the uncertainty in passive microwave snow water equivalent observations. *Remote Sensing of Environment*, *94*(2), 187–203.

Gong, G., Cohen, J., Entekhabi, D., & Ge, Y. (2007). Hemispheric-scale climate response to Northern Eurasia land surface characteristics and snow anomalies. *Global and Planetary Chang*, *56*, 359–370.

Grody, N. C., & Basist, A. N. (1996). Global identification of snow cover using SSM/I measurements. *IEEE Transactions on Geoscience and Remote Sensing*, *34*, 237–249.

Jin, R., Li, X., & Che, T. (2009). A decision tree algorithm for surface soil freeze/thaw classification over China using SSM/I brightness temperature. *Remote Sensing of Environment*, *113*, 2651–2660.

Josberger, E. G., & Mognard, N. M. (1998). Northern Great Plains snowpack hydrology from satellite passive microwave observations. *International Geoscience and Remote Sensing Symposium '98, 6–10 July, Seattle, WA, USA*.

Josberger, E. G., & Mognard, N. M. (2002). A passive microwave snow depth algorithm with a proxy for snow metamorphism. *Hydrological Processes*, *16*, 1557–1568.

Kelly, R. E. J. (2009). The AMSR-E snow depth algorithm: Description and initial results. *Journal of the Remote Sensing Society of Japan*, *29*(1), 307–317.

Kelly, R. E., Chang, A. T. C., Tsang, L., & Foster, J. L. (2003). A prototype AMSR-E global snow area and snow depth algorithm. *IEEE Transactions on Geoscience and Remote Sensing*, *41*(2), 230–242.

updated (2010). Knowles, K. W., Savoie, M. H., Armstrong, R. L., & Brodzik, M. J. (2006). *AMSR-E/Aqua daily EASE-Grid brightness temperatures from 2002 to 2010*. Boulder, Colorado USA: National Snow and Ice Data Center. Digital media.

Kuras, P. K., Weiler, M., & Alila, Y. (2008). The spatiotemporal variability of runoff generation and groundwater dynamics in a snow-dominated catchment. *Journal of Hydrology*, *352*, 50–66.

Lemmetyinen, J., Kontu, A., Kärnä, J. P., Vehviläinen, J., Takala, M., & Pulliainen, J. (2011). Correcting for the influence of frozen lakes in satellite microwave radiometer observations through application of a microwave emission model. *Remote Sensing of Environment*, *115*(12), 3695–3706.

Li, X., Nan, Z. T., Cheng, G. D., Ding, Y. J., Wu, L. Z., Wang, L. X., et al. (2011). Toward an improved data stewardship and service for environmental and ecological science data in West China. *International Journal of Digital Earth*, *4*, 347–359.

Mätzler, C. (2002). Relation between grain-size and correlation length of snow. *Journal of Glaciology*, *48*(162), 421–466.

Mätzler, C., & Wiesmann, A. (1999). Extension of the microwave emission model of layered snowpacks to coarse-grained snow. *Remote Sensing of Environment*, *70*, 317–325.

Pulliainen, J. (2006). Mapping of snow water equivalent and snow depth in boreal and sub-arctic zones by assimilating space-borne microwave radiometer data and ground-based observations. *Remote Sensing of Environment*, *101*, 257–269.

Qiu, Y. B., Shi, J. C., Lemmetyinen, J., Kontu, A., Puliainen, J., Guo, H. D., et al. (2010). The atmosphere influence to AMSR-E measurements over snow-cover areas: Simulation and experiments. *IEEE Transactions on Geoscience and Remote Sensing*, *2*, 610–613.

Ran, Y. H., Li, X., Lu, L., & Li, Z. Y. (2012). Large-scale land cover mapping with the integration of multi-source information based on the Dempster–Shafer theory. *International Journal of Geographical Information Science*, *26*(1), 169–191.

Rose, Th. (2009). RPG-4CH-DP 4 channel dual polarisation radiometer (18.7 GHz/36.5 GHz). *Test Report by Th. Rose, Radiometer Physics GmbH, 53340 Meckenheim, Germany*.

Saraf, A. K., Foster, J. L., Singh, P., & Tarafdar, S. (1999). Passive microwave data for snow-depth and snow-extent estimations in the Himalayan Mountains. *International Journal of Remote Sensing*, *20*(1), 83–95.

Simic, A., Fernandes, R., Brown, R., Romanov, P., & Park, W. (2004). Validation of VEGETATION, MODIS, and GOES+SSM/I snow cover products over Canada based on surface snow depth observations. *Hydrological Processes*, *18*, 1089–1104.

Stankov, B. B., Cline, D. W., Weber, B. L., Gasiewski, A. J., & Wick, G. A. (2008). High-resolution airborne polarimetric microwave imaging of snow cover during the NASA cold land processes experiment. *IEEE Transactions on Geoscience and Remote Sensing*, *46*, 3672–3693.

Sturm, M., Holmgren, J., & Liston, G. E. (1995). A seasonal snow cover classification-system for local to global applications. *Journal of Climate*, *8*(5), 1261–1283.

Takala, M., Luojus, K., Pulliainen, J., Derksen, C., Lemmetyinen, J., Kärnä, J. P., et al. (2011). Estimating northern hemisphere snow water equivalent for climate research through assimilation of space-borne radiometer data and ground-based measurements. *Remote Sensing of Environment*, *115*, 3517–3529.

Tanasienko, A. A., Yaktina, O. P., & Chumbaev, A. S. (2011). Effect of snow amount on runoff, soil loss and suspended sediment during periods of snowmelt in Southern West Siberia. *Catena*, *87*(1), 45–51.

Tedesco, M., & Kim, E. J. (2006). Intercomparison of electromagnetic models for passive microwave remote sensing of snow. *IEEE Transactions on Geoscience and Remote Sensing*, *44*, 2654–2666.

Tedesco, M., & Narvekar, P. S. (2010). Assessment of the NASA AMSR-E SWE product. *IEEE Transactions on Geoscience and Remote Sensing*, *3*(1), 141–159.

Tsang, L., Chen, C. -T., Chang, A. T. C., Guo, J. J., & Ding, K. -H. (2000). Dense media radiative transfer theory based on quasicrystalline approximation with applications to passive microwave remote sensing of snow. *Radio Science*, *35*(3), 731–749.

Tsutsui, H., Koike, T., & Graf, T. (2007). Development of a dry-snow satellite algorithm and validation at the CEOP reference site in Yakutsk. *Journal of the Meteorological Society of Japan*, *85A*, 417–438.

Vachon, F., Goita, K., De Seve, D., & Royer, A. (2010). Inversion of a snow emission model calibrated with in situ data for snow water equivalent monitoring. *IEEE Transactions on Geoscience and Remote Sensing*, *48*, 59–71.

Wiesmann, A., & Mätzler, C. (1999). Microwave emission model of layered snowpacks. *Remote Sensing of Environment*, *70*(3), 307–316.

Wiesmann, A., Mätzler, C., & Weise, T. (1998). Radiometric and structural measurements of snow samples. *Radio Science*, *33*(2), 273–289.